J. Fluid Mech. (1989), *vol.* 209, *pp.* 335–357
Printed in Great Britain

Chaotic advection by laminar flow in a twisted pipe

By SCOTT W. JONES†, ORAN M. THOMAS AND HASSAN AREF‡

Department of Applied Mechanics and Engineering Science,
University of California at San Diego, La Jolla, CA 92093, USA

(Received 8 March 1988 and in revised form 30 May 1989)

The appearance of chaotic particle trajectories in steady, laminar, incompressible flow through a twisted pipe of circular cross-section is demonstrated using standard dynamical systems diagnostics and a model flow based on Dean's perturbation solutions. A study is performed to determine the parameters that control fluid stirring in this mixing device that has no moving parts. Insight into the chaotic dynamics are provided by a simple one-dimensional map of the pipe boundary onto itself. The results of numerical experiments illustrating the stretching of material lines, stirring of blobs of material, and the three-dimensional trajectories of fluid particles are presented. Finally, enhanced longitudinal particle dispersal due to the coupling between chaos in the transverse direction and the non-uniform longitudinal transport of particles is shown.

1. Introduction

The phenomenon that a simple Eulerian velocity field may generate a chaotic response in the distribution of a Lagrangian marker, previously termed *chaotic advection* (Aref 1984), has been verified in several flows ranging from idealized models (thermal convection in a periodic box: Arter 1983; 'blinking vortex' flow: Aref 1984; Khakhar, Rising & Ottino 1986; Beltrami flow solutions of the three-dimensional Euler equation, e.g. ABC flows: Hénon 1966; Dombre *et al.* 1986; 'pulsed source/sink' flow: Jones & Aref 1988) to more realistic laboratory and observational situations ('driven cavity/extruder' flow: Chien, Rising & Ottino 1986; 'journal bearing' flow: Aref & Balachandar 1986; Chaiken *et al.* 1986, 1987; tidal channel oceanography: Zimmerman 1986). In spite of the solid theoretical foundation of the phenomenon and the obvious general applicability to the stirring of fluids, the subject of chaotic advection is still in need of specific flow examples where this unconventional mixture of fluid kinematics and the theory of dynamical systems can be elucidated and explored. The use of simple models in the early papers on the subject may suggest a limited range of applicability of the concepts, an inference that we certainly wish to dispel. In particular, efficient stirring by steady, laminar flow in three dimensions is an important topic that covers a wide spectrum of applications and raises new issues at a fundamental level in the theory of dynamical systems (see Feingold, Kadanoff & Piro 1988).

In this paper we suggest how chaotic advection of a passive scalar in steady laminar flow through a sequence of pipe bends leads to enhanced transverse and

† Also affiliated to Scripps Institution of Oceanography.

‡ Also affiliated to Institute of Geophysics and Planetary Physics, and San Diego Supercomputer Center.

longitudinal stirring. This type of flow is of importance to applications such as heat and mass transfer in piping systems (Kalb & Seader 1972; Prusa & Yao 1982), and to aspects of bioengineering and physiological fluid mechanics (Weissman & Mockros 1968; Chang & Tarbell 1985). We perform a parametric study of a certain model flow (discussed in §2) to explore the factors governing stirring efficiency in a pipe consisting of a sequence of bends.

It has been known since the pioneering work of Arnol'd and Hénon (1966) that steady three-dimensional flows may give rise to chaotic streamlines. Indeed, the Lagrangian equations for the passive advection of particles in three dimensions:

$$\dot{x} = u(x, y, z); \quad \dot{y} = v(x, y, z); \quad \dot{z} = w(x, y, z), \tag{1a, b, c}$$

where the dot denotes a time derivative, are rich enough in general to yield chaotic solutions. A common misconception is that the coincident streamlines and pathlines in such steady flows are closed curves or are confined to smooth surfaces. The numerical study by Hénon (1966), subsequently amplified by Dombre *et al.* (1986), using a Beltrami flow solution of the three-dimensional Euler equations showed that this is not at all the case. Indeed, only if $\boldsymbol{\omega} \times \boldsymbol{V}$ is non-vanishing everywhere, will the coincident pathlines and streamlines be confined to one of the family of Lamb surfaces (Lamb 1878; Serrin 1959) perpendicular to this vector.

The case of two-dimensional unsteady flow is formally even simpler (Aref 1984). In the case of an incompressible fluid we have the equations

$$\dot{x} = -\frac{\partial \psi}{\partial y}; \quad \dot{y} = \frac{\partial \psi}{\partial x}. \tag{2a, b}$$

These are in the form of Hamilton's canonical equations for a system with one degree of freedom. The conjugate variables are x and y, the coordinates of the advected marker particle. The Hamiltonian is the stream function ψ. All these observations are independent of the momentum equation governing the fluid motion. Thus, Hamiltonian mechanics, and the associated possibility of chaotic motion when ψ is time dependent, pertains even to the kinematics of a viscous fluid.

In this paper we consider advection by steady, three-dimensional flow through a sequence of pipe bends of circular cross-section. We shall see that although formally a problem of the type described in (1), much of the insight from investigations of time-dependent flows of the type in (2) pertains to fluid advection in this case. For clarity we shall use the term *curved* to denote a section of a pipe that has a constant radius of curvature and lies in a plane. A curved pipe is part of a torus. A *twisted* pipe will denote a pipe that consists of curved pipe segments that are not all in the same plane. It is well known that in a curved pipe segment fluid inertia leads to the formation of two longitudinal vortices of opposite sign (see the review by Berger, Talbot & Yao (1983) where many further references may be found). The flow geometry that we envision is a twisted pipe composed of a series of segments curved through 180°. The twist arises because the plane of curvature of each subsequent curved pipe segment forms an angle relative to the preceding segment. In the simplest case we have just two segments with an angle between the second and the first, and this 'basic cell' is then repeated to make up the entire twisted pipe (the two-segment basic cell is shown in figure 1). We may also consider twisted pipes with more complicated basic cells. We refer to the twist angle between the two curved pipe segments in our basic cell as the *pitch angle* of the twisted pipe and denote it χ. We utilize the following sign convention in defining the pitch angle. When following the pipe in the direction of the flow, rotation of the pipe segments in the counter-

clockwise sense increases χ. Given the diameter and radius of curvature of the curved pipe segments, the geometry of the pipe is fully prescribed when the pitch angle is given. If the pitch angle $\chi = 0°$, the twisted pipe degenerates to a torus (and one 'basic cell' suffices). If the pitch angle $\chi = 180°$, the basic cell of the twisted pipe becomes S-shaped. In both these cases the twisted pipe is confined to a plane.

The most interesting cases arise when the pipe geometry, and thus the sequence of secondary flow patterns to which an advected particle is subjected, is more complicated. In each segment, the transverse flow consists of a pair of counter-rotating vortices. For a general pitch angle the symmetry planes of the secondary flows in successive bends will not coincide, and a particle being transported along the pipe will experience a sequence of transverse flows that may be heuristically described as a 'blinking vortex dipole' flow. From earlier experiences with unsteady two-dimensional model flows (Aref 1984; Khakhar, Rising & Ottino 1986) it appears inevitable that this will create chaotic particle motion in the cross-stream direction. This will be illustrated in detail later.

The organization of the remainder of the paper is as follows: In §2 we state the mathematical model of the flow field used in our numerical experiments on advection. This is a perturbation series approximation to the real flow. We discuss various issues related to the accuracy and physical realism of our representation of the flow. In §3 we report numerical experiments on advection using the model developed in §2. In the first part of §3 we compute and consider the intersections spaced by a basic cell of individual particle tracks. We conduct a parametric study in which the flow rate and the pitch angle are varied. In this way a 'global' view of the role of chaotic advection in cross-stream transport is obtained. Then we investigate properties of a mapping of the pipe contour onto itself, 'induced' by the flow in the twisted pipe. Fixed points of this mapping on the pipe wall appear to have an important controlling influence on the cross-stream chaos within the pipe. We also compute the associated manifolds. Next, we study the stretching and stirring of 'blobs' and lines of particles. Results of this type will be important for comparison with experiments. The deformation of material lines by the full three-dimensional flow is related to the manifold structure of the two-dimensional mapping of the pipe cross-section onto itself explored earlier in the section plots, but not as simply as one might think owing to the role of the longitudinal flow. In the final part of §3 we explore this three-dimensional structure, and we present results on the coupling between cross-stream advection and the longitudinal dispersion of particles. These results suggest links to recent work on 'chaotic scattering' and a purely deterministic counterpart to Taylor's (1953) notion of shear dispersion. The latter topic is pursued in greater detail in an independent paper by Jones & Young (1989). Finally, §4 provides a discussion of our results and comments on extensions.

Previews of these results have been given on numerous occasions: see, for example, Aref & Jones (1987) and Jones, Thomas & Aref (1987). For popular introductions to the problem area of chaotic advection the reader may wish to consult Aref, Jones & Thomas (1988) or Ottino (1989).

2. Governing equations

Derivation of an approximate velocity field for flow in a curved pipe follows the seminal analysis by Dean (1927, 1928). Here we briefly outline Dean's development in order to establish our notation (see Berger *et al.* 1983 for additional material). The equations of motion are written in a toroidal coordinate system illustrated in

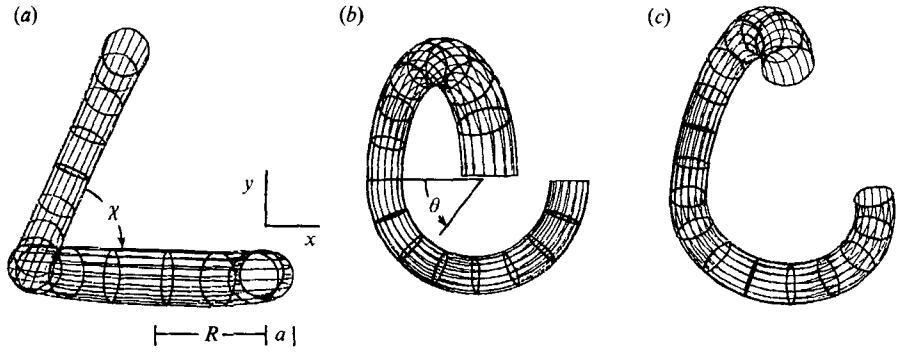

FIGURE 1. Perspective drawings of the periodic 'basic cell' used in this study composed of two 180° curved pipe segments with constant radius of curvature. The transverse coordinates x and y and the angle θ used to describe the flow in a curved pipe segment are indicated. The basic geometry is given by the pipe radius a, the radius of curvature of a bend R, and the pitch angle χ.

figure 1. The flow is assumed steady, incompressible, and all velocity components are taken to be independent of θ. Polar coordinates r, ϕ are introduced in the transverse (x, y)-plane according to $x = r\sin\phi, y = r\cos\phi$. The main perturbation assumption is that the radius of the pipe, a, is small relative to its radius of curvature, R. Scaling all lengths by a, the axial velocity w by the average axial velocity W, and the stream function ψ by the kinematic viscosity ν, yields the following non-dimensional equations for w and the secondary flow stream function ψ:

$$\nabla^2 w = \frac{1}{r}\left(\frac{\partial\psi}{\partial r}\frac{\partial w}{\partial\phi} - \frac{\partial\psi}{\partial\phi}\frac{\partial w}{\partial r}\right) - C, \tag{3a}$$

$$\nabla^2\psi = \frac{1}{r}\left(\frac{\partial\psi}{\partial r}\frac{\partial}{\partial\phi} - \frac{\partial\psi}{\partial\phi}\frac{\partial}{\partial r}\right)\nabla^2\psi + 2Dw\left(\frac{\sin\phi}{r}\frac{\partial w}{\partial\phi} - \cos\phi\frac{\partial w}{\partial r}\right). \tag{3b}$$

Here C is a non-dimensional version of the overall pressure gradient driving the flow

$$C = -\frac{a^2}{RW\mu}\frac{\partial p}{\partial\theta}. \tag{4a}$$

D is a non-dimensional parameter known as the Dean number given by

$$D = \frac{W^2 a^3}{R\nu^2}, \tag{4b}$$

and

$$Re = \frac{Wa}{\nu} \tag{4c}$$

is the usual Reynolds number. The relationship between D and Re is $D = Re^2(a/R)$.

The perturbation solution arises by expanding w and ψ, see (2), in a power series in D. At lowest order we recover the usual Poiseuille flow solution for a straight pipe. The first-order equations give us the flow that we shall use for advecting particles in a single curved segment. If we introduce (x, y)-coordinates in the transverse plane,

with the x-axis along the symmetry axis of the secondary flow, the equations of motion for a particle passively advected by the flow are

$$\dot{x} = \frac{\alpha}{1152}\left\{h(r)+\frac{y^2}{r}h'(r)\right\}, \quad \dot{y} = -\frac{\alpha}{1152}\frac{xy}{r}h'(r), \quad \dot{\theta} = \tfrac{1}{4}\beta(1-r^2). \quad (5a, b, c)$$

Here $r^2 = x^2+y^2$, and (5c) is simply a Poiseuille profile for the axial flow. The prefactors α and β in (5a, b) are related to C, D and Re, equation (4), via $\alpha = DC^2$, $\beta = DC/Re$. The function $h(r)$ is given by

$$h(r) = \tfrac{1}{4}(4-r^2)(1-r^2)^2, \quad (6)$$

and $h'(r)$ is its derivative with respect to r.

Since the flow is steady, (5) are autonomous and the independent variable can be changed from time t to angle θ by simply dividing (5a, b) by (5c). This yields

$$\frac{\mathrm{d}x}{\mathrm{d}\theta} = \frac{\gamma}{1152}(4-5x^2-23y^2+x^4+8x^2y^2+7y^4), \quad \frac{\mathrm{d}y}{\mathrm{d}\theta} = \frac{\gamma}{192}xy(3-x^2-y^2), \quad (7a, b)$$

where $\gamma = \alpha/\beta$. Equation (7) defines the mapping of fluid particles from one cross-sectional plane θ = constant to another due to the flow in the curved pipe. Higher-order approximations are available but we shall be content with this one for our work here (see additional discussion below).

It is important to distinguish the actual time-evolving advection described by (5) from the 'induced' mapping of the cross-section given by (7). Equation (5) is divergence-free in the sense that

$$\frac{\partial\dot{x}}{\partial x}+\frac{\partial\dot{y}}{\partial y} = 0, \quad (8a)$$

which simply reflects the incompressibility of the flow. The system defined by (7), on the other hand, does not share this property. Indeed, if one calculates

$$\frac{\partial}{\partial x}\left(\frac{\mathrm{d}x}{\mathrm{d}\theta}\right)+\frac{\partial}{\partial y}\left(\frac{\mathrm{d}y}{\mathrm{d}\theta}\right) \quad (8b)$$

it is seen to be non-zero. Hence, (7) leads to a mapping of the cross-section that is not area-preserving. This is not very important, however, because we may introduce a rescaled radial coordinate R given by

$$R(r) = r(1-\tfrac{1}{2}r^2)^{\frac{1}{2}}, \quad (9)$$

and in the (R,ϕ)-coordinates the mapping (7) is area-preserving. An outline of the calculation leading to (9) is given in the Appendix.

Of more significance is the difference in physical interpretation of (5) and (7). Since the time has been scaled out, (7) does not contain the important information that fluid particles at the pipe wall make no progress along the pipe owing to the no-slip boundary condition. Indeed, according to (7) points on the pipe boundary slip along it (formally owing to cancellation of the $1-r^2$ factor between (6) and (5c). This cancellation must always occur according to boundary-layer theory; see Aref *et al.* 1989). Equation (7) may be thought of as a kind of $t\to\infty$ limit of the flow given by (5). We shall explore the features of the mapping of the invariant pipe boundary onto itself in §3.1, and return to additional points regarding the usefulness of diagnostics pertaining to the two-dimensional mapping (7) when addressing particle advection in the fully three-dimensional flow in the pipe in §3.4.

The flow of particles in a twisted pipe with a pitch angle χ is now represented by

a sequence of Dean solutions, augmented by a rotation of the particles through an angle $-\chi$ between successive segments. Letting M represent the mapping between successive cross-sections given by (7) and T be a rotation of fluid particles by $-\chi$, the mapping of the two-segment basic cell in figure 1 has the symbolic representation A = TMTM. The mapping A has the following limits. As $\gamma \to 0$ the secondary flow vanishes and A becomes a rotation, $A = T^2$. This limit is not of much interest here. For $\chi = 0°$ the mapping is $A = M^2$ and particles are constrained to follow the secondary streamlines given by the Dean solution. Finally for $\chi = 180°$ the mapping reduces to the identity.

In addition to the usual approximations implied by a perturbation solution, our method of patching together Dean solutions makes further assumptions about the flow. First, we must assume that the flow becomes fully developed as soon as it enters the curved segment. This, we understand, is achievable experimentally to a good approximation when the flow goes from Poiseuille flow in a straight pipe to Dean flow in a single curved pipe (Berger *et al.* 1983). Second, we must assume that as we go from one curved segment to the next, the flow readjusts very quickly from one secondary flow pattern to another. This assumption is much more dubious, not to say incorrect in general. It is found that the vortex system set up in a curved pipe segment can be quite persistent (see, for example, Kao 1987). Indeed, it is well known that the secondary vortices set up in curved pipe flow can delay transition to turbulence (White 1929; Taylor 1929; Lighthill 1970). Finally, we assume that the lowest-order Dean solution is adequate in each curved segment, although higher-order approximations are available (Dean 1927, 1928; Berger *et al.* 1983).

We argue that although our flow model is probably not realistic for the pipe shown as figure 1, it can be approximated in the laboratory by inserting segments of straight pipe between the curved segments.† A straight pipe segment allows the secondary vortices set up in a bend to decay. Hence, the vortices set up in the following bend with a different axis of symmetry are decoupled. We argue, further, that the introduction of such straight segments in no way invalidates the effects we are documenting. The main flow features that are present in our model are in essence topological: we require a system of secondary vortices in each curved segment with an axis of symmetry that can be prescribed. The main point on which we rely is that the symmetry of the secondary flow between one curved segment and the next is an independent parameter, i.e. is not determined by the flow itself. We are also content to use the lowest-order Dean solution since the accuracy of this solution is governed by other parameters, in particular a/R, that we wish to be independent of the pitch angle χ for the flow regimes of interest here. The dynamical systems features that we rely on to describe the transition to chaos in the transverse motion are generic to periodically forced, near-integrable Hamiltonian systems with one degree of freedom. Hence, the accuracy of description of the spatial structure of the transverse flow should not be a major issue. We are confident that the general qualitative trends should be reproducible in a pipe flow experiment in the appropriate regimes.

We may add that we suspect advection by the 'real flow' set up in a pipe made up of cells such as the one shown in figure 1 to be chaotic, but we may not capture even a qualitatively correct picture of this using the present model. We expect that our model results in this paper are more likely to be valid for real flows at small values of the pitch angle χ than as χ approaches 180°. The reason is easy to see. For

† This is the approach adopted in the one experimental set-up of which we are aware due to Professor C. D. Andereck at Ohio State University.

$\chi = 180°$ the model flow leads to every point being returned to its original position after each basic cell, since whatever transverse motion the first curved bend produces, the second bend will undo. This is only possible if the two secondary flows in successive curved segments of a real pipe have been entirely decoupled.

3. Numerical experiments

3.1. *Transverse stirring: Poincaré sections*

To demonstrate chaotic particle motion in the transverse direction we use the standard dynamical systems diagnostic known as the Poincaré section. To construct Poincaré sections the positions of particles are tracked as they advect down the pipe and their location in the pipe cross-section is plotted after each basic cell. Operationally, (7) is numerically integrated for prescribed initial conditions through 180° using a fifth-order Fehlberg Runge–Kutta method. The particle positions are then rotated through $-\chi$, the integration is repeated and the particles are rotated again to recover the initial orientation.

Once the basic cell has been specified the two parameters that govern the subsequent flow are γ and χ. Poincaré sections are presented in figures 2–4 illustrating the influence that these two parameters have on the flow. In all Poincaré sections the initial conditions are chosen to highlight the structure of the regular regions. Each initial condition is iterated through 1000 periodic units. This is, of course, not practical for a real pipe and is simply done in order to map out the Poincaré section. Effects of the chaotic motion may be seen after only a few bends. Figures 2 and 3 show the effect of varying χ while γ is held constant for two different values of γ. For $\chi = 0°$ the system is integrable and the Poincaré section reproduces the secondary streamlines of Dean flow (figure 2*a*). As χ deviates from 0° for fixed γ the size of the regular region diminishes. It is interesting to note that the dipole vortex structure of the integrable torus case dominates the regular region of the sections, with the chaotic paths being confined to a band across the middle of the pipe and along the walls. For $\gamma = 100$ there appears to be a 'most chaotic geometry' at about $\chi = 90°$. Increasing χ further approaches the S-pipe in which every point is mapped to itself. Thus the Poincaré section shows increased regularity as $\chi \to 180°$. Colour versions of figure 2(*d*, *e*) appear as figure 14(*c*, *e*) (plate 2).

In figure 4 the pitch angle χ has been fixed at 90° to explore changes in the flow due to varying γ. For a given value of χ a larger set of initial conditions follow chaotic trajectories as γ is increased. This dependence is captured in figure 4. Note that figure 2(*f*) would fit into the sequence between figure 4(*a*) and (*b*). Parameter choices with completely chaotic particle paths, as approximated in figure 4(*c*) and achievable for other parameter choices, form the basis for the work in Jones & Young (1989).

It is clear that these Poincaré sections are symmetric about a line at an angle $\frac{1}{2}\chi$ with respect to the line joining the top and bottom of the pipe. To show this formally we note that the mapping M induced by the secondary flow is symmetric with respect to reflection in the y-axis:

$$\mathrm{M}^{-1}\mathrm{R}_y = \mathrm{R}_y\mathrm{M}, \tag{10}$$

where $\mathrm{R}_y(x, y) = (-x, y)$. From elementary geometry we have

$$\mathrm{T}^{-1}\mathrm{R}_y = \mathrm{R}_y\mathrm{T}. \tag{11}$$

Thus, if $\mathrm{S} = \mathrm{TR}_y$, i.e. reflection in the line rotated $\frac{1}{2}\chi$, and $\mathrm{A}' = \mathrm{TM}$,

$$(\mathrm{A}')^{-1}\mathrm{S} = \mathrm{SA}'. \tag{12}$$

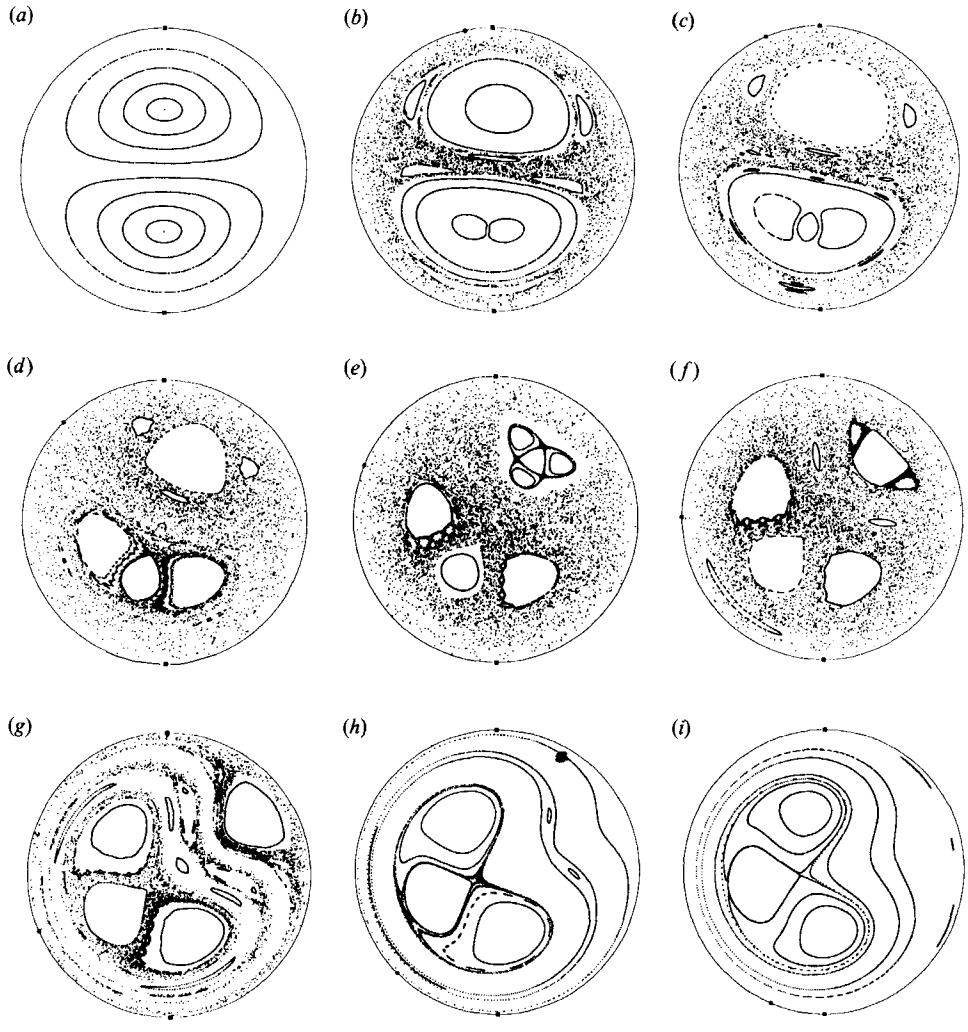

FIGURE 2. Poincaré sections showing chaotic particle motion in the transverse direction. In all panels $\gamma = 100$ and (a) $\chi = 0$; (b) $\frac{1}{16}\pi$; (c) $\frac{1}{8}\pi$; (d) $\frac{1}{4}\pi$; (e) $\frac{3}{8}\pi$; (f) $\frac{1}{2}\pi$; (g) $\frac{5}{8}\pi$; (h) $\frac{3}{4}\pi$; (i) $\frac{7}{8}\pi$.

This relation shows that the set of iterates $(A')^n P$ of some initial point P coincides with the reflection of the set of iterates of SP. Hence, any set of points that is invariant under S will produce upon iteration a set that is invariant under S. In particular, if P is a periodic point of any period, SP will be a periodic point of the same period.

3.2. *Mapping of the pipe boundary onto itself*

An invariance of a different sort arises by considering the circumference of the pipe. This circle is an invariant under the mapping A′. Thus the full mapping A induces a one-dimensional mapping of the boundary onto itself. We have investigated this mapping $A_1 = TM_1TM_1$, where M_1 is the solution of

$$\frac{d\phi}{d\theta} = -\frac{\gamma}{96}\cos\phi \tag{13}$$

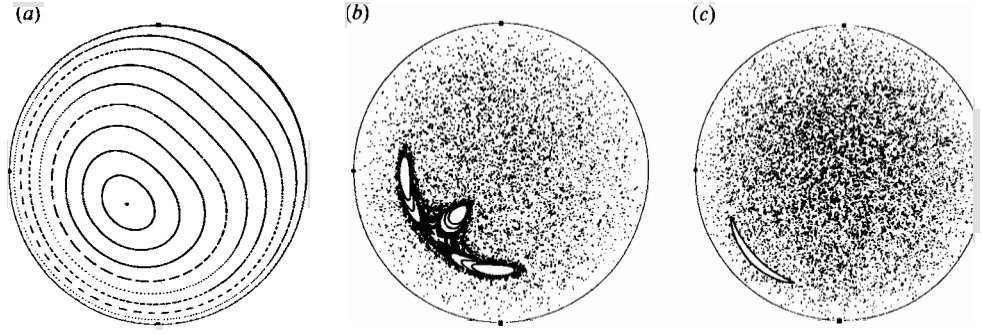

FIGURE 3. Poincaré sections for $\gamma = 200$ and (*a*) $\chi = \frac{1}{4}\pi$; (*b*) $\frac{1}{2}\pi$; (*c*) $\frac{3}{4}\pi$.

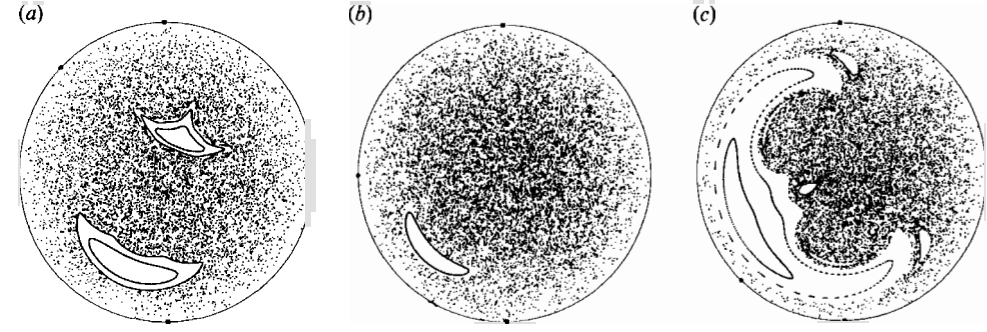

FIGURE 4. Poincaré sections for $\chi = \frac{1}{2}\pi$ and (*a*) $\gamma = 50$; (*b*) 150; (*c*) 250.

integrated from $\theta = \theta_0$ to $\theta = \theta_0 + \pi$, and A_1 is calculated modulo 2π. Equation (13) is derived by setting $r = 1$ in (7)† (or in (A 2)). Note that M_1 gives the separatrix connecting the unstable fixed points on the pipe boundary. The mapping A_1 is integrable and provides some insight into the location of the unstable fixed points responsible for the chaotic dynamics of the two-dimensional map A shown in figures 2–4. Solving (13) for ϕ_{n+1} in terms of ϕ_n yields

$$\phi_{n+1} = 2\tan^{-1}\{\Gamma \tan(\tfrac{1}{2}\phi_n + \tfrac{1}{4}\pi)\} - \tfrac{1}{2}\pi, \tag{14a}$$

where

$$\Gamma = \exp(-\pi\gamma/96). \tag{14b}$$

The mapping $A_1' = TM_1$ is given by

$$\phi_{n+1} = 2\tan^{-1}\{\Gamma \tan(\tfrac{1}{2}\phi_n + \tfrac{1}{4}\pi)\} + \chi - \tfrac{1}{2}\pi. \tag{15}$$

To be consistent with the sign convention used by Dean we must add the pitch angle at each iteration.

The fixed points of the map A_1' are found by setting $\phi_{n+1} = \phi_n = \phi^*$ and solving (15). This gives

$$\phi^* = 2\tan^{-1}\left(\frac{1-\Gamma \pm [(1-\Gamma)^2 - 4\Gamma\tan^2(\frac{1}{2}\chi)]^{\frac{1}{2}}}{2\Gamma\tan\frac{1}{2}\chi}\right) - \tfrac{1}{2}\pi. \tag{16}$$

† We recall that the polar coordinates are such that $x = r\sin\phi$, $y = r\cos\phi$, and ϕ increases clockwise (from $\phi = 0$ along the positive y-axis, cf. figure 1).

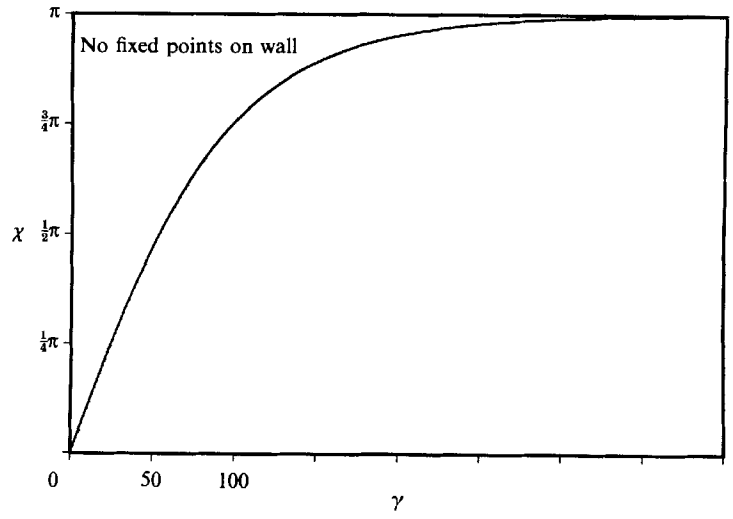

FIGURE 5. Graph of the dividing curve for the condition (17). The region beneath the curve satisfies the inequality.

For fixed γ or Γ, (14*b*), there will be two solutions to (16), i.e. two fixed points on the pipe wall, for all pitch angles χ for which the argument of the square root in (16) is positive, i.e. in view of (14*b*) for which

$$\tan \tfrac{1}{2}\chi \leqslant \sinh \frac{\pi\gamma}{192} \tag{17}$$

(see figure 5). Since the left-hand side grows beyond all bounds as $\chi \to \pi$, it follows that there cannot be fixed points on the boundary for all values of the pitch angle. On the other hand, the full mapping $A' = TM$ of the disk onto itself is continuous, and therefore must have at least one fixed point by the theorem of Brouwer (cf. Courant & Robbins 1941, ch. v, §3.4 for an elementary exposition). In general there are fixed points within the disk well before the condition (17) is violated (cf. figure 2).

For very large γ the parameter Γ is small, and we may expand the solutions ϕ^* in powers of Γ. We then find that one fixed point (the stable one) is always close to $\frac{1}{2}\pi$, the other (unstable fixed point) is close to $\chi - \frac{1}{2}\pi$. Indeed, it is easy to see in general from (16) that the two values given by this equation satisfy

$$\phi_+^* + \phi_-^* = \chi, \tag{18}$$

so that these two fixed points are symmetrically situated with respect to the symmetry axis of the Poincaré section at $\phi = \frac{1}{2}\chi$, as must be the case according to our previous general discussion in (12).

3.3. *A global view of the Poincaré sections*

The parametric dependence of the two fixed points on the boundary, and their approach as $\chi \to \pi$, together with the symmetry of the Poincaré section suggests a global picture of the emergence of large-scale chaos in this system. The boundary fixed points are saddle points as far as the mapping of the disk onto itself is concerned. In the integrable case $\chi = 0$, i.e. the torus, their nature and location defines the topology of the transverse flow (figure 2*a*). As χ is increased chaos arises

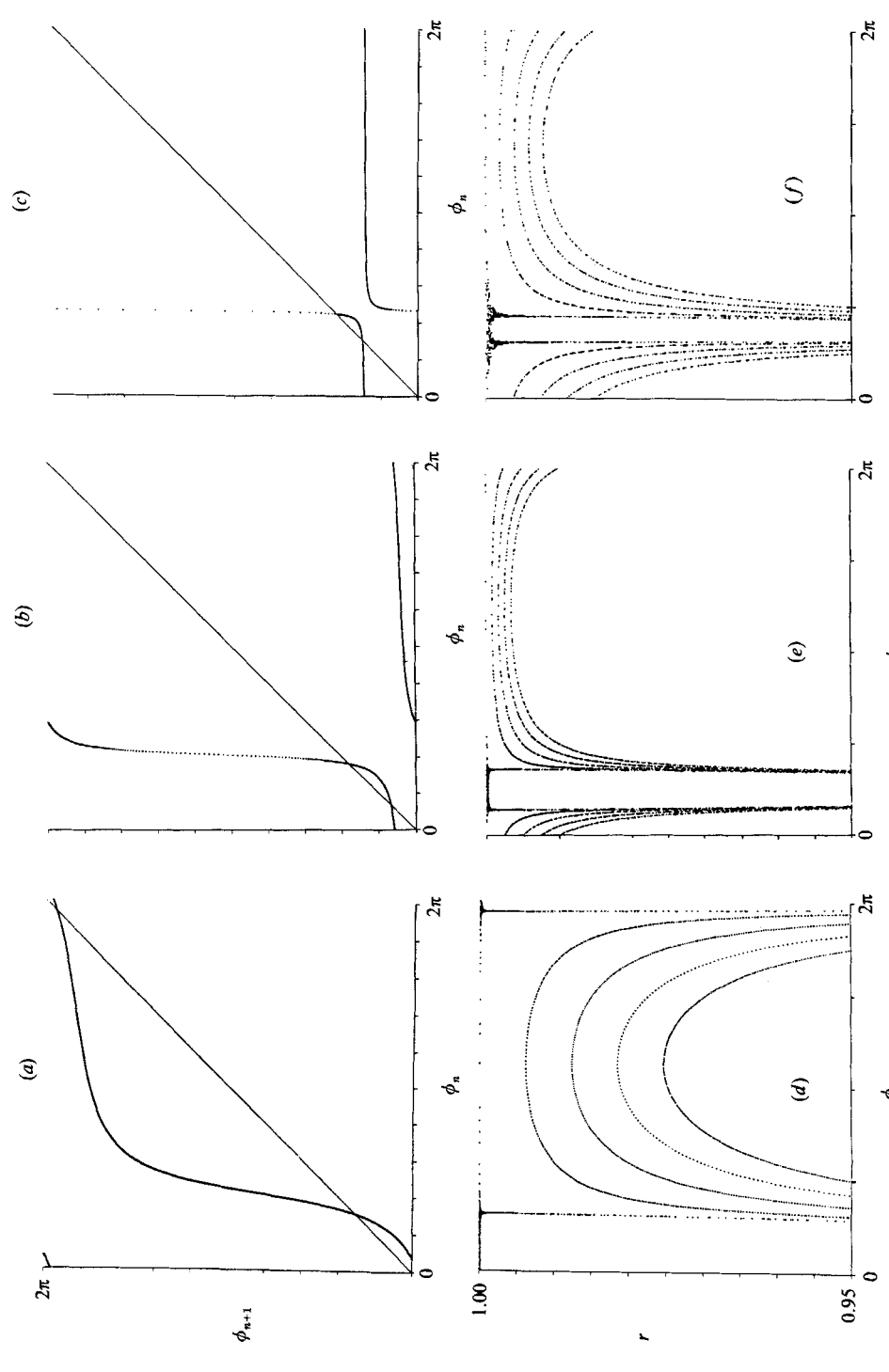

FIGURE 6. The one-dimensional map of the pipe boundary onto itself (*a–c*) and Poincaré sections of the boundary region $0.95 \leqslant r \leqslant 1$ (*d–f*). (*a, d*) $\chi = \frac{1}{4}\pi$, $\gamma = 30$; (*b, e*) $\frac{1}{2}\pi$, 60; (*c, f*) $\frac{3}{4}\pi$, 110. Note the correspondence between the location in ϕ of fixed points (*a–c*) and the vertical lines in the (r, ϕ)-plot (*d–f*) representing a manifold.

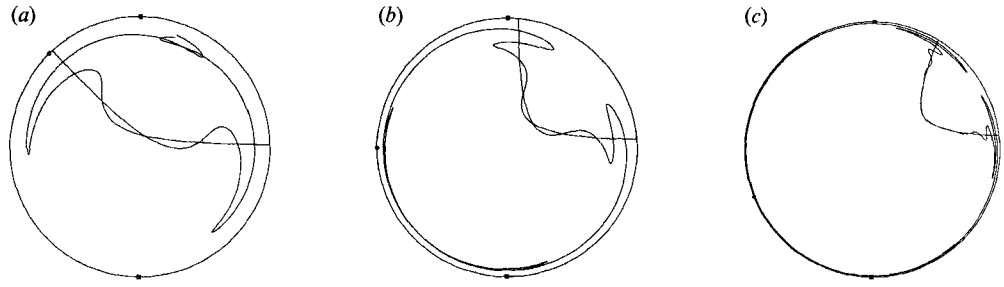

FIGURE 7. Stable and unstable manifolds corresponding to the hyperbolic fixed points of (7) on the pipe wall. Parameters are $\gamma = 100$ and (a) $\chi = \frac{1}{4}\pi$; (b) $\frac{1}{2}\pi$; (c) $\frac{5}{8}\pi$.

immediately because the saddle connection from one to the other is disrupted leading to a so-called 'heteroclinic tangle' (see Moser 1973; Lichtenberg & Lieberman 1983 for a description). Figure 6(*a–c*) shows samples of the boundary circle mapping (14) for three different values of γ and χ. The two fixed points are clearly seen as the intersections between the graph ϕ_{n+1} versus ϕ_n and the line $\phi_{n+1} = \phi_n$. The slope at the stable (unstable) fixed point is <1 (>1). Also shown (figure 6*d–f*) are Poincaré sections of a thin circular annulus in the boundary region $0.95 \leqslant r \leqslant 1$. The annulus has been 'unfolded' and plotted in an (r, ϕ)-diagram. For small χ the homoclinic oscillations that arise from the disruption of the saddle connection, connecting opposite sides of the pipe boundary in the integrable $\chi = 0°$ case, are an important 'global' feature of the flow. For large χ, on the other hand, the fixed points of the mapping A_1 are close together on the pipe boundary, and A_1 fails to capture much of the chaotic behaviour of A. For example, figure 6(*c,f*) shows the fixed points for the map A_1 at $\gamma = 110$ and $\chi = \frac{3}{4}\pi$, a case that is very similar to figure 2(*h*). At this value of γ the advection in the heteroclinic tangle of the stable and unstable manifolds connected to the fixed points of A_1 is confined to a thin layer at the boundary. Most of the chaotic stirring arises from an unstable fixed point close to the centre of the pipe.

Figure 7 provides a different view. Here we show the computed manifolds belonging to the unstable fixed points of (7) on the pipe boundary. Note that because we are using the r-coordinate in the radial direction the mapping is not area-preserving and the lobes between stable and unstable manifolds do not have the same area. For a case such as figure 7(*a*), where the pitch angle is small, the manifolds do yield insight into the overall structure of the Poincaré section. For cases such as figure 7(*c*), where the pitch angle is much larger, these manifolds are confined to a relatively small region of the pipe cross-section.

3.4. *Stretching of material interfaces*

We next illustrate the stretching of a material line. The rate of stretching has been shown to be closely related to the Lyapunov exponent (Khakhar & Ottino 1986), which gives the exponential rate of divergence of neighbouring trajectories. Although we have not explicitly calculated Lyapunov exponents for these models flows, the chaotic regions of the Poincaré sections are strong evidence that a positive Lyapunov exponent exists. Recall that in (7) the independent variable is θ rather than t. We shall use (7) to calculate stretching even though it contains no temporal information. Figures 8 and 9 show the 'evolution' via (7) of a line of particles initially situated as a diameter of the pipe cross-section with a $\frac{1}{2}\chi$ rotation from the horizontal. After a

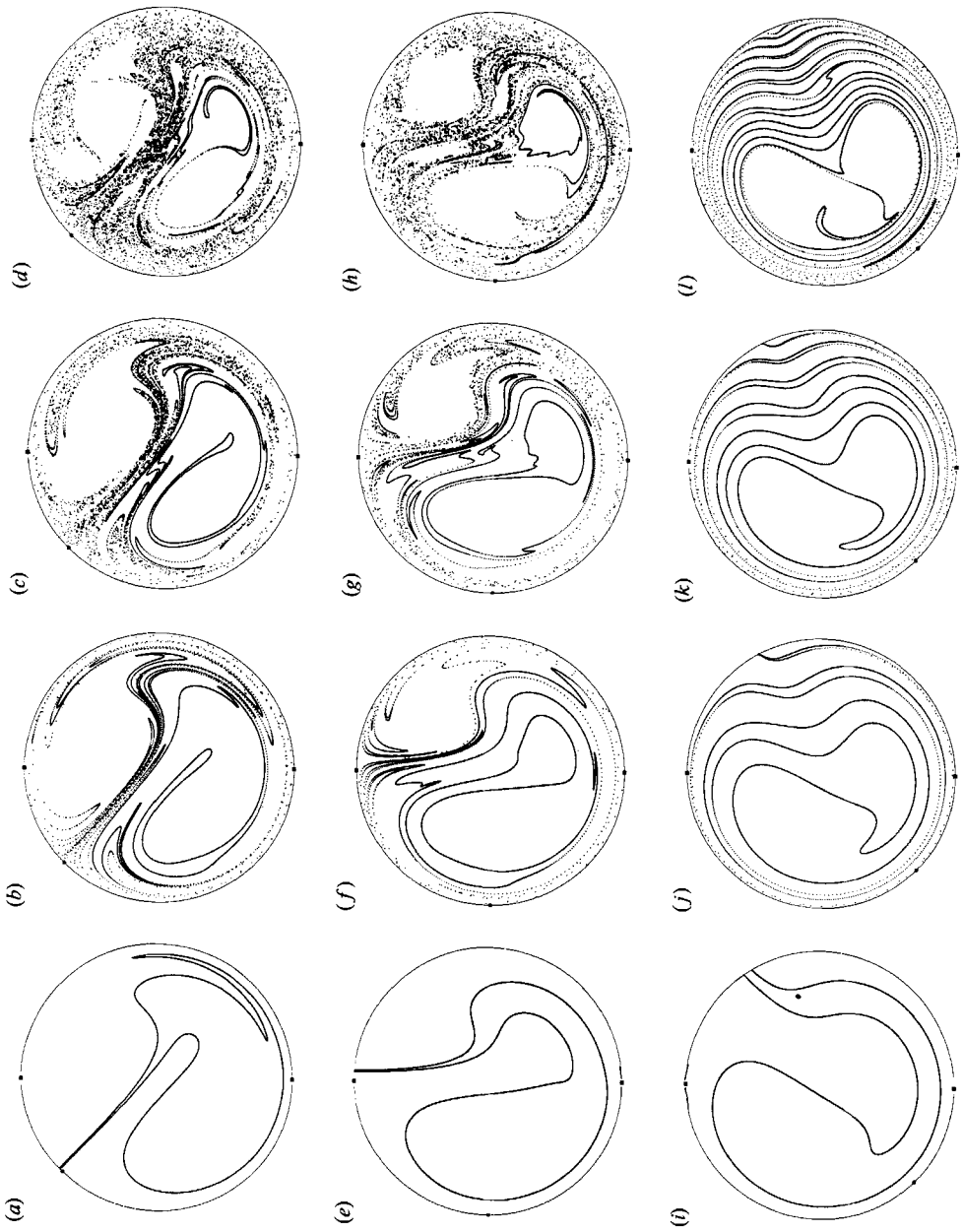

FIGURE 8. Stretching of material lines. In all panels $\gamma = 100$. Along each row the pitch angle is the same: (*a–d*) $\chi = \frac{1}{4}\pi$; (*e–h*) $\frac{1}{2}\pi$; (*i–l*) $\frac{3}{4}\pi$. The number of basic cells that the line has been advected through (i.e. the number of iterations of the mapping) is constant down each column and increases from left to right. First column, $N = 1$; second, 3; third, 5; fourth, 10.

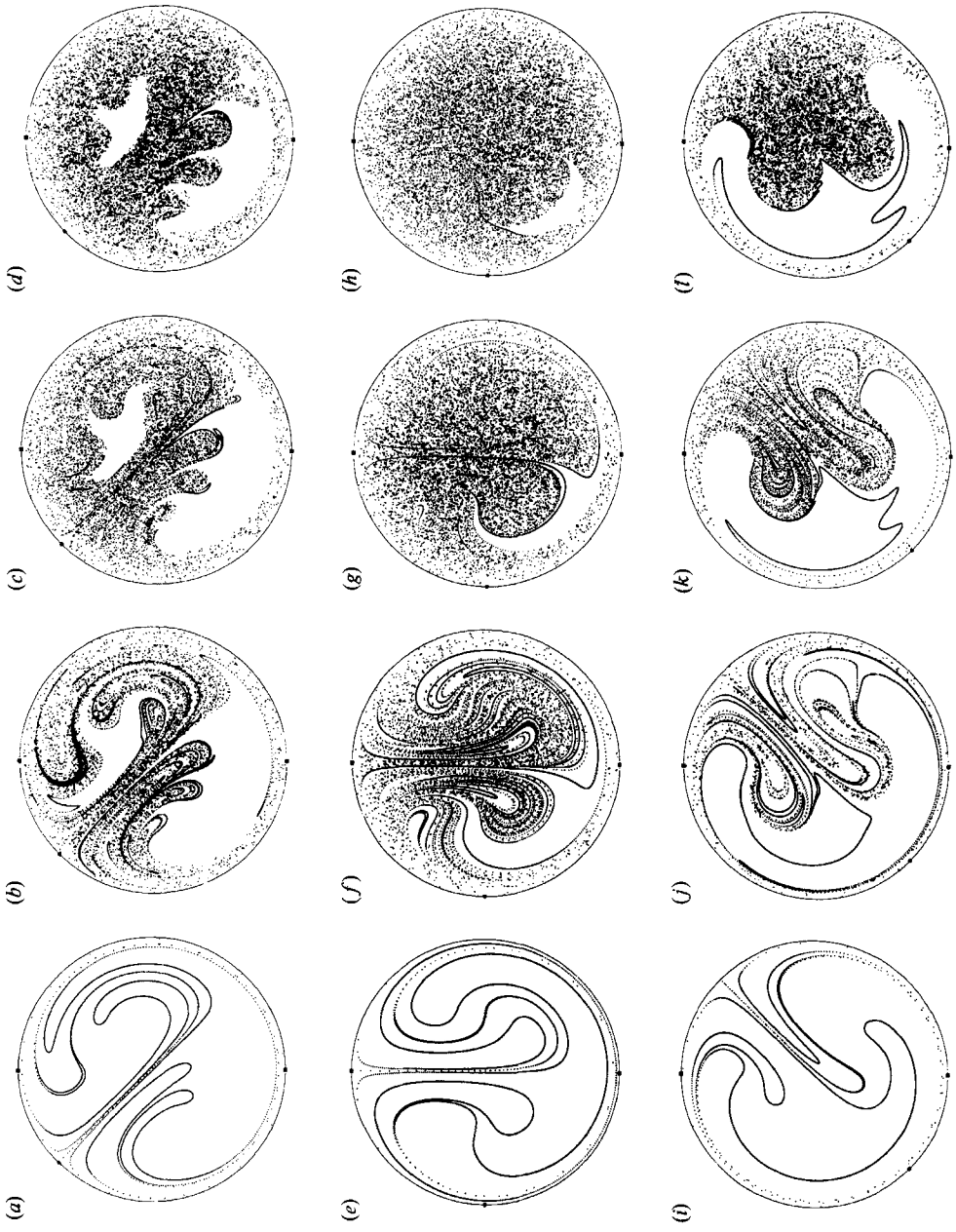

FIGURE 9. Stretching of material lines. In all panels $\gamma = 200$, otherwise all parameter values are identical to figure 8.

single iteration the points of intersection with the boundary have been swept to the vicinity of the unstable fixed point, as must happen owing to the character of the mapping A_1 as displayed in figure 6(*c*). The line has been significantly stretched and shows 'tendrils' (Berry *et al.* 1979), i.e. wiggles due to the oscillations of manifolds (see figure 7) associated with the unstable hyperbolic fixed point on the boundary. This stretching process continues in subsequent iterations (figure 8). After about ten basic cells the structure of the corresponding Poincaré section begins to appear.

These distributions of advected particles are not attainable in a real flow starting with just one line of marker particles since, as mentioned above, the mapping (7) that we use is not identical to the governing equations of advection, i.e. (5). The particles of the initial line do not all arrive at a given pipe cross-section at the same time. However, if marker particles are continuously fed in along the diagonal used as the initial condition in figure 8, then after a sufficiently long time the patterns seen in later panels of this figure will appear at a fixed location along the pipe. (Equivalently, a long time exposure of the cross-section can be used if only a single line of marker particles is introduced.) Indeed, the main difference between the stochastic patterns seen in chaotic advection, and the superficially similar patterns that would be seen instantaneously in a turbulent pipe flow is that the chaotic advection patterns at a given cross-section are completely stationary in time. Thus, with continuous fixed feed at the inlet the patterns in the first column of figure 8 or 9 (panels *a*, *e*, *i*) will be seen after one basic cell, those in the second column (panels *b*, *f*, *j*) after three basic cells, etc. It is instructive to compare figure 8(*d*) to figure 7(*a*) and figure 2(*d*) and, similarly, to compare 8(*h*) to 7(*b*) and 2(*f*).

3.5. *Transient effects*

The stirring of collections of particles in chaotic regions of the flow differs profoundly from the stirring of particles trapped within regular regions (cf. figure 10 of Jones & Aref 1988). In addition to this obvious distinction there are more subtle transient effects on the stirring of particles entirely within chaotic regions.

One of the most important transient effects on the stirring of particles entirely within chaotic regions is the presence of 'cantori'. A cantorus possesses a cantor-set-like structure and acts as a leaky barrier to particle transport (Mackay, Meiss & Percival 1984). Blobs of particles stirred within regions bounded by cantori can be confined for some initial period but eventually some of the particles will escape from this region and explore more of the chaotic region. Such escape would, of course, be impossible from within a KAM surface. The stirring of a small circle filled with 5000 particles, and placed within what we believe is a cantorus, is shown in figure 10. The parameter values for this flow are $\gamma = 100$ and $\chi = \frac{1}{2}\pi$. After 25 iterations (or basic cells; figure 10*b*) the circle has been stretched around the three lower islands apparent in the corresponding Poincaré section (figure 2*f*) but no particles have escaped from this immediate area. After 50 iterations (figure 10*c*) a handful of particles have leaked through the cantorus. After 100 iterations (figure 10*d*) several hundred particles have escaped.

The presence of a cantorus is easily visualized when the initial positions and iterates of a particle are colour-coded. In figure 11 (plate 1) a single red particle is placed initially inside the cantorus shown in figure 10, and a pale blue particle is placed outside the cantorus. Both particles are iterated 2000 times and the iterates are coloured the same as the initial position. Eventually the red particle escapes; however, the blue particle has not penetrated the cantorus. (Clearly such effects are

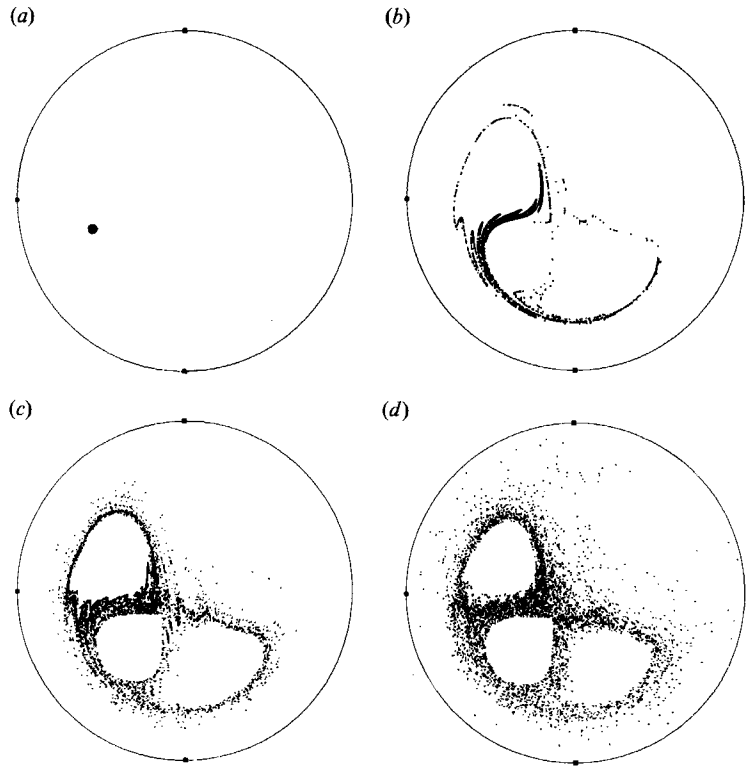

FIGURE 10. Transient stirring of a circular blob placed within a cantorus for $\chi = \frac{1}{2}\pi$, $\gamma = 100$. (a) Initial positions; (b) after 25 basic cells; (c) 50; (d) 100.

obscured in Poincaré sections such as figure 2.) The cantorus is at the border between the region of predominately red dots and the region composed of a mixture of red and blue dots in figure 11.

A related transport feature is illustrated in figure 12(*a*, *b*) (plate 1). Here we are concerned with transport of particles from the interior of the pipe volume to the wall region, a crucial feature for applications in heat and mass transfer. We have used a technique pursued elsewhere (Aref *et al.* 1989) in which positions in the domain are colour-coded according to the time it takes a particle starting there to reach a specified target region, in this case a strip of thickness one-tenth the radius near the pipe wall. Figure 12(*a*) shows the intuitively obvious results for integrable advection in the torus geometry. The only particles to reach the wall at all are located within the streamline pattern formed by that particular streamline which passes within a distance of $0.1a$ of the wall.

For a non-integrable case, on the other hand, these rigid barriers are broken and many more initial locations of particles now lead to transport to the wall region. This is illustrated in figure 12(*b*). The black region (particles that take a very long time to reach the wall, and probably never make it) is much smaller and has a highly convoluted, probably fractal boundary.

The intuitive message from figure 12 is that chaotic transverse advection leads to enhanced transport to the wall region, and this is amplified by figure 13 which provides histograms of the number of particles arriving in the wall region as a function of time for the two cases. For figure 12(*a*), the integrable case, one sweep of

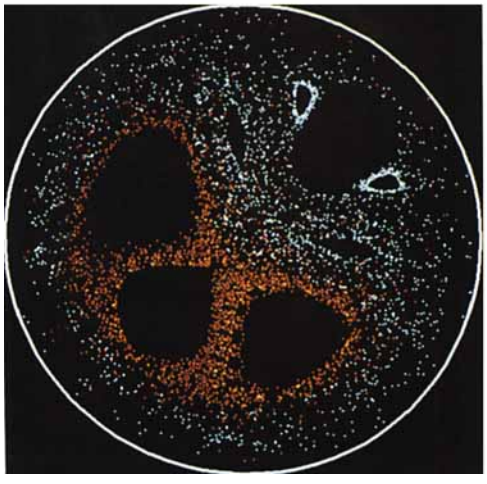

FIGURE 11. Poincaré section indicating position of a cantorus for $\chi=\frac{1}{2}\pi$, $\gamma=100$.

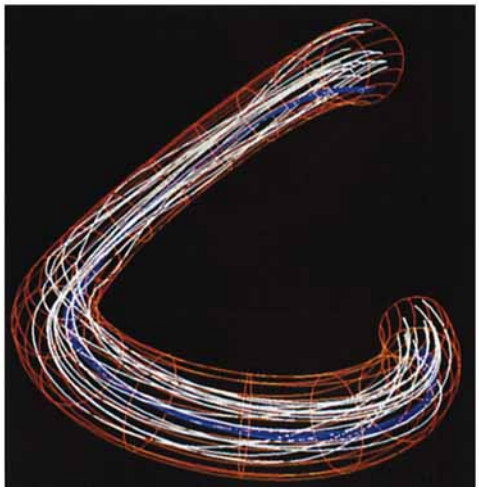

FIGURE 15. Streamline or particle path (white) in the chaotic region for $\chi=\frac{1}{4}\pi$, $\gamma=250$.

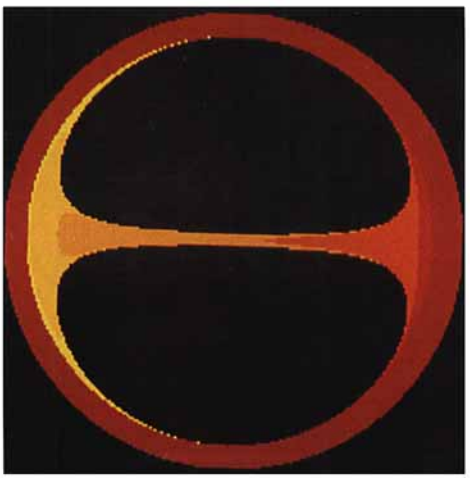

FIGURE 12. Time of arrival in the wall region for particle initial positions in the cross-section: *(a)* integrable case, $\gamma=200$, $\chi=0$; *(b)* non-integrable case, $\gamma=200$, $\chi=\frac{1}{2}\pi$. The colour coding is such that short arrival times are deep red, with longer times in the orange, yellow and white. Particle positions that never make it to the wall region are coloured black.

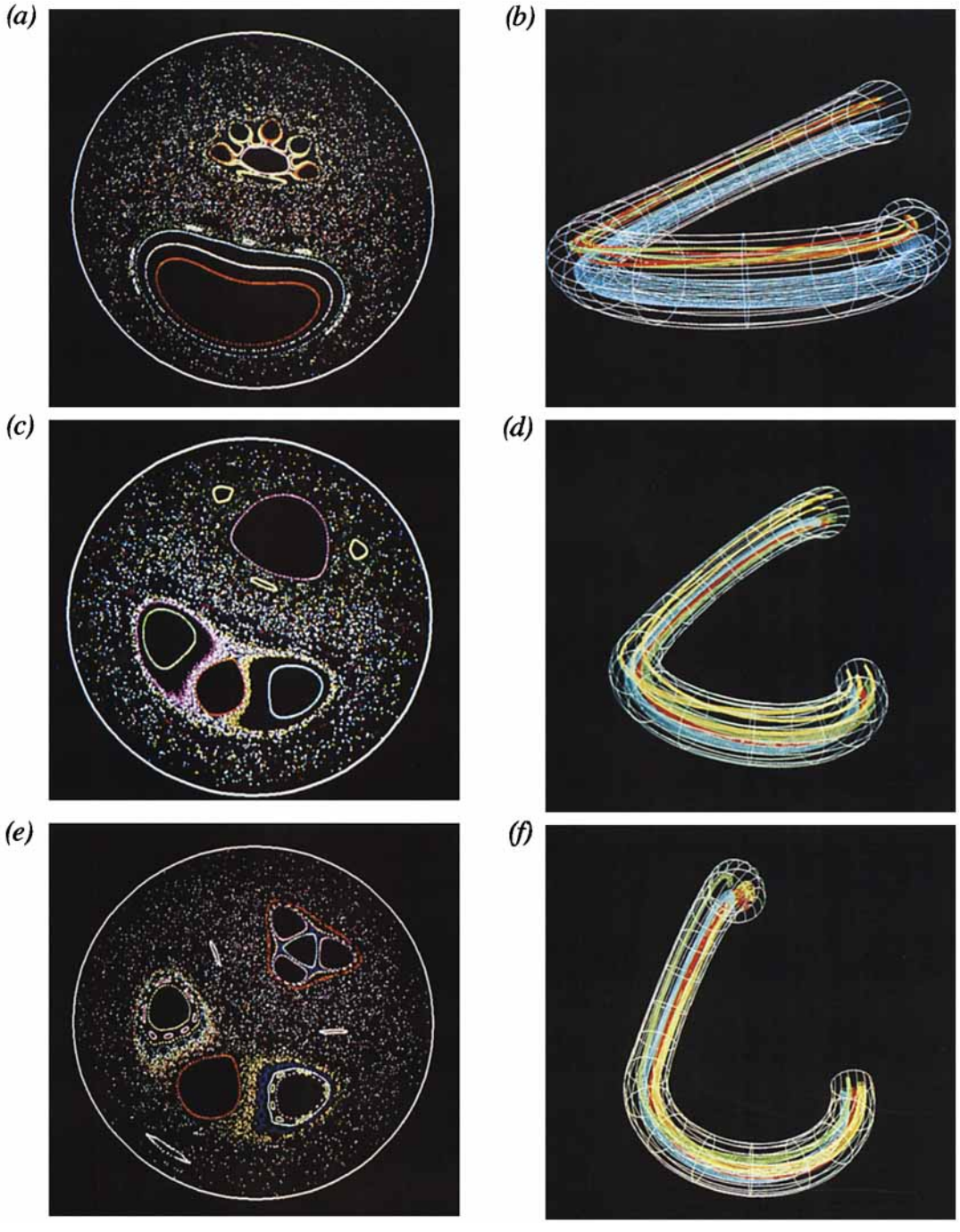

FIGURE 14. *(a)* Poincaré section for $\chi=\frac{1}{8}\pi$, $\gamma=200$. *(b)* Streamlines or particle paths with same parameter values as *(a)*. Streamlines are colour-coded to correspond to the iterates in the Poincaré section. *(c)* Poincaré section for $\chi=\frac{1}{4}\pi$, $\gamma=100$. *(d)* Streamlines or particle paths corresponding to *(c)*. *(e)* Poincaré section for $\chi=\frac{3}{8}\pi$, $\gamma=100$. *(f)* Streamlines or particle paths corresponding to *(e)*.

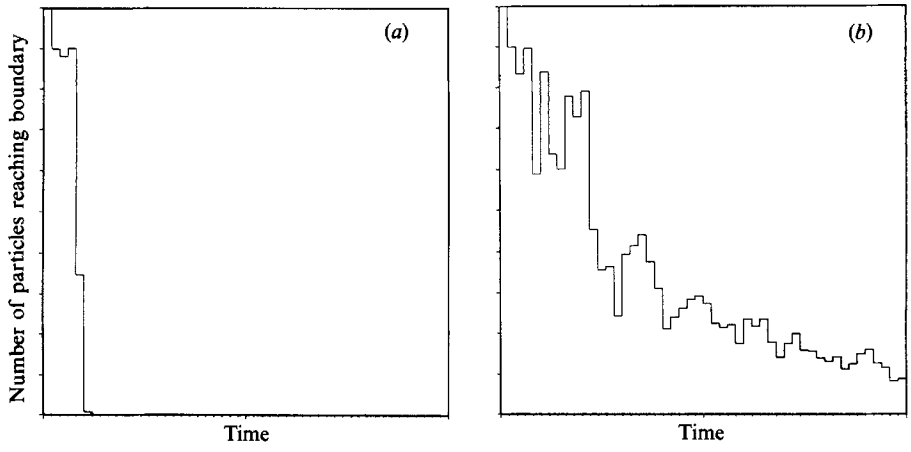

FIGURE 13. Histograms of number of particles arriving in the wall region as a function of time for the two cases shown in figure 12.

finite duration accounts for all the transport. For figure 12(*b*), on the other hand, many more particles ultimately arrive at the wall, and there is a long time tail in the distribution. We believe that these simple calculations show that chaotic advection is an essential control mechanism for enhancing transport to the wall region. This is very important in a variety of applications.

3.6. *Three-dimensional structure and longitudinal dispersion*

Thus far we have examined the chaotic advection of particles in the cross-sectional plane, i.e. we have largely been dealing with the two-dimensional system in (7). However, the flow considered is three-dimensional and manifestations of chaotic behaviour should be apparent in the longitudinal dispersion† of advected particles as well. To get an impression of the three-dimensionality of the motion we first present corresponding pictures of Poincaré sections and of streamlines of the flow using a 'periodic basic cell'. To facilitate the comparison we have colour-coded the streamlines to correspond with the iterates in the Poincaré section. Figure 14(*a–f*) (plate 2) give examples of such Poincaré section–streamline pairs. In these figures we have drawn only streamlines corresponding to regular motion. For such cases, a net-like structure of streamlines densely covers the surface of a streamtube (figure 14*b*, *d*, *f*). On the other hand for a streamline or pathline in the chaotic region, as shown in figure 15 (plate 1), an erratic pattern emerges. Within each curved section the streamlines in both chaotic and regular regions are, of course, smooth. In regular regions, however, the streamlines wind around the streamtube in a regular helical motion, while in chaotic regions the motion from cell to cell appears uncorrelated. We also draw attention to the intertwined tubes arising from periodic points in the Poincaré section. For example, in figure 14(*b*) we see the intertwining of three yellow and three blue tubes associated with the two sets of period-3 points in the section. In figure 14(*d*) a similar effect is seen for the three white tubes associated with the period-3 point. These tubes of flow suggest that it is possible to inject fluid in a

† We use the word 'dispersion' for the rapid separation of neighbouring tracer particles. This includes the conventional use of the word for the growth rate of the variance in a diffusion process, but applies also to cases of 'anomalous diffusion' as one observes in systems of the present kind.

twisted tube in such a way that it does not become mixed with the ambient fluid, and travels down the pipe in its own well-defined channel. Results of this type may be useful for considerations regarding drug delivery by injection.

The subject of longitudinal dispersion of a scalar in pipe flow has received considerable attention since the seminal analysis by Taylor (1953). In his analysis Taylor demonstrated, within certain assumptions, that the longitudinal dispersion of a diffusing scalar obeys a diffusion equation in a reference frame moving with the mean axial velocity. The effective diffusion coefficient for this longitudinal dispersion is inversely related to the transverse diffusivity. We do not, of course, have any diffusion in our problem. However, as we have seen, the possibility of chaotic motion may be likened to a diffusion process, and this suggests that we look at the longitudinal distribution of particles in our model twisted pipe flow. This problem is considered further by Jones & Young (1989).

In the case of a diffusing, advected scalar the effect of the secondary flow has been found to reduce the longitudinal dispersion (Erdogan & Chatwin 1967; Nunge, Lin & Gill 1972; Janssen 1976; Johnson & Kamm 1986). These results, however, all pertain to the case of integrable transverse motion. Here we show that considerable longitudinal dispersion of a non-diffusing scalar can be produced by the coupling between a chaotic transverse flow and the longitudinal flow. To illustrate this 10000 particles, numbered sequentially, are positioned along a diameter of the pipe. The diameter is chosen as the axis of symmetry of the corresponding Poincaré section (cf. figure 2). Each particle index uniquely labels the Lagrangian initial coordinate. Equation (5) is now integrated for a fixed amount of time and the final longitudinal position (i.e. value of the angle θ) of each particle is plotted versus its index. The results of such calculations are shown in figure 16 for six different choices of γ and χ. At early times (the lowest curve in each panel of figure 16) we see smooth curves with the entire longitudinal dispersion being due to the difference in velocity at the pipe centre and the boundary. At later times, however, increasing structure is visible in the graphs plotted. We now see collections of particles that show little longitudinal dispersion interrupted by particles that show considerable longitudinal dispersion, and adjacent particles have dramatically different final longitudinal positions. The data in these plots appear similar to data from chaotic scattering problems (cf. Noid, Gray & Rice 1986; Eckhardt 1988).

By comparing figure 16(*a–c*) to figure 2(*d, f, h*) we see that the smoothly varying parts of the graphs in figure 16 correlate with the regular islands of the corresponding Poincaré sections. The interpretation of this observation is that the particles within an island of the Poincaré section participate in a regular winding motion in the transverse plane. As we saw in figure 14(*b, d, f*) they wind along the pipe in a regular, quasi-periodic fashion. Hence, they all make much the same progress along the pipe in a given interval of time. In this sense their fate is similar to the trivial problem of non-diffusive advection in Poiseuille flow in a straight pipe. In the chaotic regime, on the other hand, particles sample many different longitudinal velocities as they go from segment to segment along the pipe. Figure 15 provided a view of the trajectory of such particles. Furthermore, particles started very close to one another will have substantially different longitudinal velocity histories because their sampling of transverse positions will show a sensitive dependence on initial position. Thus, particles in these regions will show considerable longitudinal dispersion as is clearly seen in figure 16(*a, b, d–f*). Figure 16(*c*) corresponds to the predominantly regular Poincaré section in figure 2(*h*). Chaotic transverse motion, therefore, can lead to enhanced longitudinal dispersion relative to the integrable case. This is an intriguing

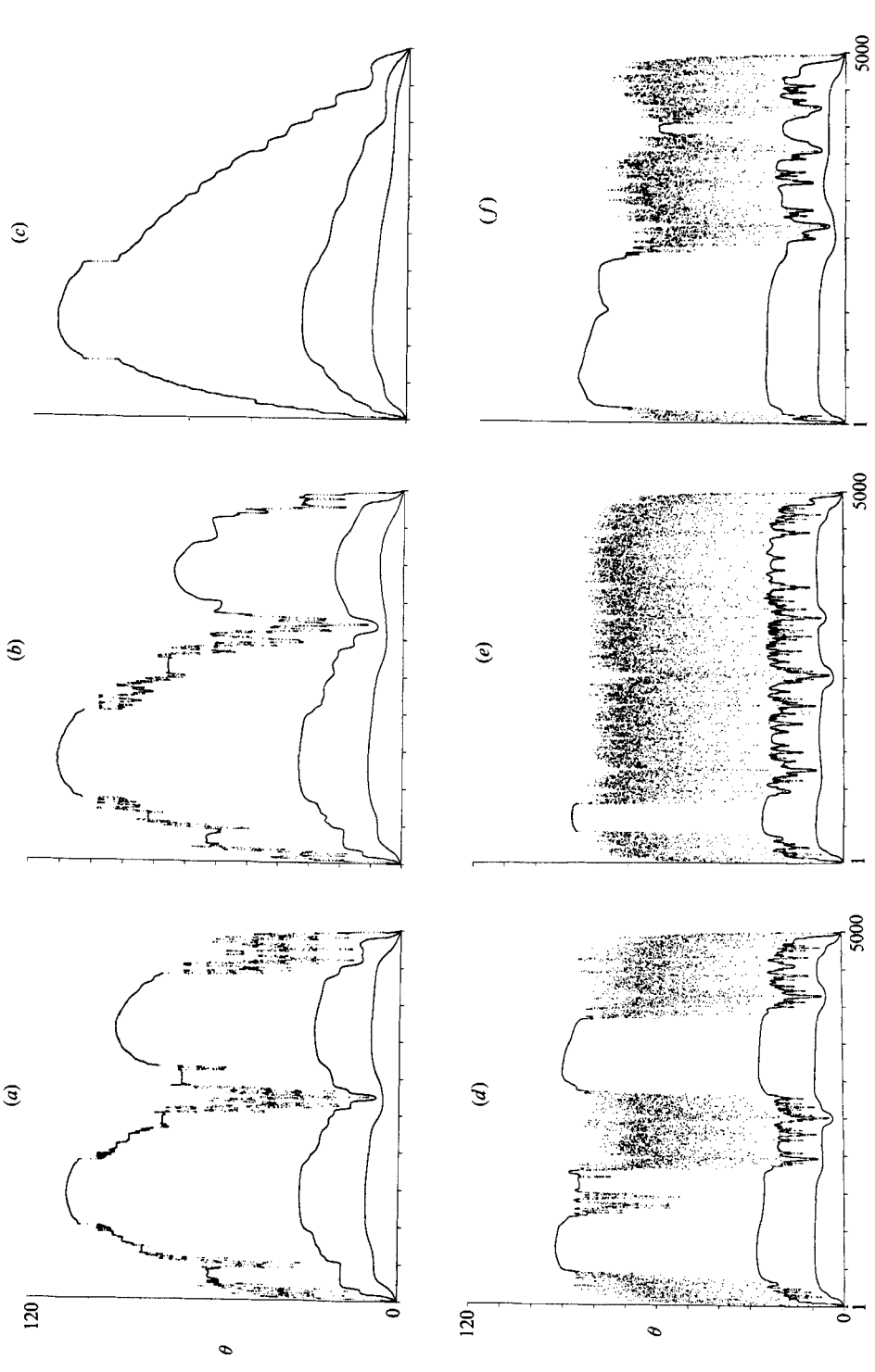

FIGURE 16. Longitudinal dispersion of particles. Abscissae are particle indices (1–5000) in the initial state. Ordinates are axial progression measured in radians along the twisted pipe. (*a–c*) are for $\gamma = 100$ and time increases from curve to curve (bottom to top). (*a*) $\chi = \frac{1}{4}\pi$; (*b*) $\frac{1}{2}\pi$; (*c*) $\frac{3}{4}\pi$; (*d–f*) are for $\gamma = 200$ and again the top 'curve' is for the latest time. (*d*) $\chi = \frac{1}{4}\pi$; (*e*) $\frac{1}{2}\pi$; (*f*) $\frac{3}{4}\pi$.

result because in a first approximation chaotic motion is sometimes modelled as a diffusion process (Lichtenberg & Lieberman 1983) and so we have a deterministic analogue of Taylor's shear dispersion mechanism. (The full elucidation of this interesting phenomenon requires considerable additional work, and we must refer the reader to the sequel paper by Jones & Young 1989.)

The fractal structure seen in figure 16, similar to the scattering data of non-integrable scattering problems, has implications for residence time distributions in chaotically advecting flows and suggests a new area of application for chaotic scattering or 'chattering' as it is called (cf. Eckhardt 1988).

4. Conclusion

We have suggested via a parametric study of advection by certain model flows that chaotic stirring of particles will take place for laminar flow in a twisted pipe. The flow model that we have used contains several approximations that are difficult to assess. We look forward to the problem being addressed experimentally in the near future.

The practical implication of chaotic particle trajectories is that they enhance stirring quality. This enhancement of stirring quality is achieved without requiring any additional energy input to the system, or any additional expenditure of force. This is because the transition from integrable to chaotic particle motion is a kinematical effect, fundamentally different in nature from the transition from laminar to turbulent flow. The latter in general does require an increase in the amount of energy used to agitate the fluid. In the example discussed here we show how the transition from regular to chaotic particle motion can be achieved by modifying only the geometry of our pipe. The stirring is always achieved by a laminar flow, and the subtle changes in geometry should not require an increase in the overall pressure drop required to drive the fluid through the pipe. (In the model the geometry can, of course, be changed independently of the pressure drop.) An appropriately designed twisted pipe provides an intriguing example of an efficient fluid stirring device without moving parts. It differs from the static mixers in that it utilizes fluid inertia to set up the secondary flow.

Although the approximations inherent in our description of the flow disqualify us from precise quantitative statements, our results do give qualitative guidelines on how to 'tune' the geometry of a real pipe for maximum stirring efficiency. Consider first the pitch angle χ. As mentioned previously, for $\chi = 0°$ and $\chi = 180°$ the flow is regular and material lines are stretched at a rate that is linear in time. However, small deviations from $\chi = 0°$ apparently have a more profound impact on stirring than a comparable deviation from $\chi = 180°$ for a given value of γ (see figure 2 and compare $\chi = \frac{1}{4}\pi$ to $\chi = \frac{3}{4}\pi$). The efficiency of devices such as heat exchangers and blood oxygenators relies on scalar transport to the pipe boundary. This is enhanced by stirring in the boundary region. Thus, the chaotic behaviour for χ near 0° is more beneficial to the efficient operation of such devices than that for χ near 180°.

Our results suggest that transverse transport is enhanced when condition (17) is met. This should translate into greater heat exchange between the fluid in the pipe and the ambient. Thus, it should be possible to lead fluid through two twisted pipe flows in a bath of a fixed temperature and obtain different degrees of cooling (or heating) at the outlet for fixed value of γ, simply by constructing the two pipes with different values of χ!

We have only presented results from the simple basic cell composed of two

segments (figure 1). We have also studied a four-segment basic cell given by the mapping

$$A = T^{-1}MT^{-1}MTMTM,$$

although not in as much detail as the two-segment case. It appears from this preliminary study that, as the geometry of the basic cell becomes more complex, chaotic particle trajectories are more easily generated. Obviously, many more modifications to the pipe geometry are possible. We are satisfied that even with the simplest geometry we have captured the essential features necessary to produce efficient stirring in this steady, three-dimensional, laminar flow.

This work was supported by DARPA/URI grant N00014-86-K-0758 administered by ONR, by NSF/PYI award MSM84-51107, and by IGPP/LANL grant 88-16-215. Computer resources provided at the San Diego Supercomputer Center were invaluable.

Appendix

We show how to arrive at (9) for the scaled radial coordinate. From (7), $x = r\sin\phi$, $y = r\cos\phi$, we obtain the polar coordinate versions of (7):

$$\frac{dr}{d\theta} = \frac{\gamma}{1152}(1-r^2)(4-r^2)\sin\phi, \tag{A 1}$$

$$r\frac{d\phi}{d\theta} = \frac{\gamma}{1152}\{(1-r^2)(4-r^2)-6r^2(3-r^2)\}\cos\phi. \tag{A 2}$$

We wish to introduce $R(r)$ such that

$$\frac{1}{R}\frac{\partial}{\partial R}\left(R\frac{dR}{d\theta}\right)+\frac{\partial}{\partial\phi}\left(\frac{d\phi}{d\theta}\right) = 0. \tag{A 3}$$

Let us seek a 'stream function' $\psi(R,\phi) = -(\gamma/1152)F(R)\cos\phi$ such that

$$\frac{dR}{d\theta} = \frac{1}{R}\frac{\partial\psi}{\partial\phi}; \quad R\frac{d\phi}{d\theta} = -\frac{\partial\psi}{\partial R}. \tag{A 4}$$

Then by the chain rule $dR/d\theta = R'\,dr/d\theta$, where R' is dR/dr, and using (A 1), (A 2) we obtain two relations for F:

$$F(R) = RR'(1-r^2)(4-r^2), \tag{A 5a}$$

$$\frac{dF}{dR} = \frac{R}{r}\{(1-r^2)(4-r^2)-6r^2(3-r^2)\}. \tag{A 5b}$$

These give

$$d(R^2) = \frac{2F\,dr}{(1-r^2)(4-r^2)} = \frac{2r\,dF}{(1-r^2)(4-r^2)-6r^2(3-r^2)}. \tag{A 6}$$

From the last two of these $F(r)$ may be found, and then $R(r)$ is determined. We shall not give the tedious intermediate calculations but simply state the results:

$$F(r) = r(1-r^2)^2(4-r^2), \tag{A 7}$$

$$R(r) = r(1-\tfrac{1}{2}r^2)^{\frac{1}{2}}. \tag{A 8}$$

The reader may easily verify that (A 4) is satisfied.

REFERENCES

AREF, H. 1984 Stirring by chaotic advection. *J. Fluid Mech.* **143**, 1–21.

AREF, H. & BALACHANDAR, S. 1986 Chaotic advection in a Stokes flow. *Phys. Fluids* **29**, 3515–3521.

AREF, H. & JONES, S. W. 1987 Chaotic advection: Efficient stirring of viscous liquids. In *Proc. Fifth Symp. Energy Engin. Sci., Argonne Nat. Lab. CONF*-8706187, pp. 209–216.

AREF, H., JONES, S. W., MOFINA, S. & ZAWADZKI, I. 1989 Vortices, kinematics and chaos. *Physica* D **37**, 423–440.

AREF, H., JONES, S. W. & THOMAS, O. M. 1988 Computing particle motions in fluid flows. *Computers in Phys. (USA)* **2** (6), 22–27.

ARTER, W. 1983 Ergodic stream-lines in steady convection. *Phys. Lett.* A **97**, 171–174.

BERGER, S. A., TALBOT, L. & YAO, L.-S. 1983 Flow in curved pipes. *Ann. Rev. Fluid Mech.* **15**, 461–512.

BERRY, M. V., BALAZS, N. L., TABOR, M. & VOROS, A. 1979 Quantum maps. *Ann. Phys.* **122**, 26–63.

CHAIKEN, J., CHEVRAY, R., TABOR, M. & TAN, Q. M. 1986 Experimental study of Lagrangian turbulence in a Stokes flow. *Proc. R. Soc. Lond.* A **408**, 165–174.

CHAIKEN, J., CHU, C. K., TABOR, M. & TAN, Q. M. 1987 Lagrangian turbulence and spatial complexity in a Stokes flow. *Phys. Fluids* **30**, 687–694.

CHANG, L.-J. & TARBELL, J. M. 1985 Numerical simulation of fully developed sinusoidal and pulsatile (physiological) flow in curved tubes. *J. Fluid Mech.* **161**, 175–198.

CHIEN, W.-L., RISING, H. & OTTINO, J. M. 1986 Laminar mixing and chaotic mixing in several cavity flows. *J. Fluid Mech.* **170**, 355–377.

COURANT, R. & ROBBINS, H. 1941 *What is Mathematics? An Elementary Approach to Ideas and Methods.* Oxford University Press, 521 pp.

DEAN, W. R. 1927 Note on the motion of fluid in a curved pipe. *Phil. Mag.* **4**, 208–223.

DEAN, W. R. 1928 The streamline motion of fluid in a curved pipe. *Phil. Mag.* **5**, 673–693.

DOMBRE, T., FRISCH, U., GREENE, J. M., HÉNON, M., MEHR, A. & SOWARD, A. M. 1986 Chaotic streamlines in the ABC flows. *J. Fluid Mech.* **167**, 353–391.

ECKHARDT, B. 1988 Irregular scattering. *Physica* D **33**, 89–98.

ERDOGAN, M. E. & CHATWIN, P. C. 1967 The effects of curvature and buoyancy on the laminar dispersion of solute in a horizontal tube. *J. Fluid Mech.* **29**, 465–484.

FEINGOLD, M., KADANOFF, L. & PIRO, O. 1988 Passive scalars, three-dimensional volume-preserving maps, and chaos. *J. Statist. Phys.* **50**, 529–565.

HÉNON, M. 1966 Sur la topologie des lignes de courant dans un cas particulier. *C. R. Acad. Sci. Paris* **262**, 312–314.

JANSSEN, L. A. M. 1976 Axial dispersion in laminar flow through coiled tubes. *Chem. Engng Sci.* **31**, 215–218.

JOHNSON, M. & KAMM, R. D. 1986 Numerical studies of steady flow dispersion at low Dean number in a gently curving tube. *J. Fluid Mech.* **172**, 329–345.

JONES, S. W. & AREF, H. 1988 Chaotic advection in pulsed source–sink systems. *Phys. Fluids* **31**, 469–485.

JONES, S. W., THOMAS, O. M. & AREF, H. 1987 Chaotic advection by laminar flow in a twisted pipe. *Bull Am. Phys. Soc.* **32**, 2026.

JONES, S. W. & YOUNG, W. R. 1989 Shear dispersion and anomalous diffusion by chaotic advection. *J. Fluid Mech.* (submitted).

KALB, C. E. & SEADER, J. D. 1972 Heat and mass transfer phenomena for viscous flow in curved circular tubes. *Intl J. Heat Mass Transfer* **15**, 801–817.

KAO, H. C. 1987 Torsion effect on fully developed flow in a helical pipe. *J. Fluid Mech.* **184**, 335–356.

KHAKHAR, D. V., FRANJIONE, J. G. & OTTINO, J. M. 1987 A case study of chaotic mixing in deterministic flows: the partitioned pipe mixer. *Chem. Engng Sci.* **42**, 2909–2926.

KHAKHAR, D. V. & OTTINO, J. M. 1986 Fluid mixing (stretching) by time periodic sequences for weak flows. *Phys. Fluids* **29**, 3503–3505.

KHAKHAR, D. V., RISING, H. & OTTINO, J. M. 1986 Analysis of chaotic mixing in two model systems. *J. Fluid Mech.* **172**, 419–451.

LAMB, H. 1878 On the conditions for steady motion of a fluid. *Proc. Lond. Math. Soc.* **9**, 91–92.

LICHTENBERG, A. J. & LIEBERMAN, M. A. 1983 *Regular and Stochastic Motion.* Springer.

LIGHTHILL, M. J. 1970 Turbulence. In *Osborne Reynolds and Engineering Science Today* (ed. D. M. McDowell & J. D. Jackson), pp. 83–146. New York: Barnes & Noble.

MACKAY, R. S., MEISS, J. D. & PERCIVAL, I. C. 1984 Transport in Hamiltonian systems. *Physica* D **13**, 55–81.

MOSER, J. 1973 *Stable and Random Motions in Dynamical Systems.* Princeton University Press.

NOID, D. W., GRAY, S. K. & RICE, S. A. 1986 Fractal behavior in classical collisional energy transfer. *J. Chem. Phys.* **51**, 363–383.

NUNGE, R. J., LIN, T.-S. & GILL, W. N. 1972 Laminar dispersion in curved tubes and channels. *J. Fluid Mech.* **51**, 363–383.

OTTINO, J. M. 1989 The mixing of fluids. *Sci. Am.* **260**, 56–67.

PRUSA, J. & YAO, L.-S. 1982 Numerical solution for fully developed flow in heated curved tubes. *J. Fluid Mech.* **123**, 503–522.

SERRIN, J. 1959 The mathematical principles of fluid mechanics. In *Handbuch der Physik*, vol. VIII/1 (ed. S. Flügge). Springer.

TAYLOR, G. I. 1929 The criterion for turbulence in curved pipes. *Proc. R. Soc. Lond.* A **124**, 243–249.

TAYLOR, G. I. 1953 Dispersion of soluble matter in solvent flowing slowly through a tube. *Proc. R. Soc. Lond.* A **219**, 186–203.

WEISSMAN, M. H. & MOCKROS, L. F. 1968 Gas transfer to blood flowing in coiled circular tubes. *Proc. ASCE Engng Mech. Div. J.* **94**, 857–872.

WHITE, C. M. 1929 Streamline flow through curved tubes. *Proc. R. Soc. Lond.* A **123**, 645–663.

ZIMMERMAN, J. T. F. 1986 The tidal whirlpool: A review of horizontal dispersion by tidal and residual currents. *Netherlands J. Sea Res.* **20**, 133–154.